Large-eddy simulation of passive-scalar mixing using multifractal subgrid-scale modeling

By G.C. Burton

1. Motivation and introduction

Turbulent mixing of a passive scalar is important to a number of processes of interest to industry and science, including multiphase flows and the dispersion of pollutants in atmospheric flows. Turbulent mixing also is of particular interest to the modeling of reacting flows, since turbulence is known to mix reactants in an extremely rapid manner, which may greatly influence the rate and efficiency of the reactive processes. While experimental and/or field work may continue to provide certain insights into the characteristics of these flows, their analysis may be difficult, time consuming or expensive to conduct. As a result, the practicing engineer and scientist has turned in the past decade to numerical simulation to develop a more detailed understanding of turbulent flows. In this context, large eddy simulation has been shown to be a promising approach to numerically simulate many turbulent flows. However, most current subgrid-scale models used for LES fail to recover the detailed spatial structure of the stress and energy transfer fields of such flows. These factors, however, may be of particular importance for modeling processes that occur principally in the subgrid scales, such as energy-dissipation, scalar-dissipation and chemical reactions.

Recently, Burton & Dahm (2004 *a,b*) have introduced multifractal modeling for large-eddy simulation, which derives a structural model for the subgrid velocities u_i^{sgs} based on the demonstrated multifractal structure of the subgrid vorticity field $\boldsymbol{\omega}^{sgs}$, and uses this to close the filtered Navier-Stokes momentum equation. The method shows special promise because, at modest computational cost, multifractal LES has been shown to recover the detailed spatial structure of the subgrid-energy production $\mathcal{P}(\mathbf{x},t)$ field with high accuracy ($\rho \geq 0.997$). Importantly the multifractal modeling approach may be applied to other turbulence modeling problems. Thus, the multifractal structure of the passive-scalar dissipation field in high Re turbulence, already confirmed by previous studies, may be used to develop a model for the filtered passive-scalar transport equation. In this report, the derivation of such a model is set out in detail, as well as *a priori* tests of the model against DNS data, and *a posteriori* tests in which the model is employed in large-eddy simulations of the turbulent mixing of a passive scalar. These tests indicate that multifractal modeling holds great promise for the accurate simulation of turbulent mixing of passive conserved scalar quantities.

2. Derivation of a multifractal model for the filtered passive-scalar flux

2.1. *Background*

For large-eddy simulation, the filtered passive-scalar transport equation without source term may be expressed as

$$\frac{\partial \overline{\zeta}}{\partial t} + \frac{\partial}{\partial x_j}\,\overline{\overline{u}_j\,\overline{\zeta}} - D\frac{\partial^2 \overline{\zeta}}{\partial x_j \partial x_j} = -\frac{\partial}{\partial x_j}\,\sigma_j^*\,, \tag{2.1}$$

where D is the coefficient of scalar diffusivity, and where

$$\sigma_j^* \equiv \overline{\overline{u}_j\, \zeta^{sgs}} + \overline{u_j^{sgs}\, \overline{\zeta}} + \overline{u_j^{sgs}\, \zeta^{sgs}}. \tag{2.2}$$

Equations (2.1) and (2.2) involve filtered nonlinear interactions between the resolved and subgrid velocities $\overline{u}_j$ and u_j^{sgs} on the one hand, and the resolved and subgrid passive-scalar concentrations $\overline{\zeta}$ and ζ^{sgs} on the other, and require some form of modeling. One approach is to evaluate the terms in σ_j^* from a structural model that provides the subgrid velocity components u_j^{sgs} and the subgrid-scalar concentrations ζ^{sgs}. Burton & Dahm (2004 *a,b*) have proposed such a model for u_j^{sgs} based on the multifractal structure of the vorticity field in high Reynolds-number turbulence. The approach involves describing the spatial distribution of subgrid vorticity magnitude by a multifractal cascade and the distribution of subgrid vorticity orientations by an additive decorrelation cascade. An expression for the subgrid velocity components can be derived by applying the Biot-Savart operator to this representation of the subgrid vorticity, which after some analysis takes the form:

$$u_j^{sgs} \approx \mathcal{B}\, u_j^{\Delta}, \tag{2.3}$$

where

$$\mathcal{B} \equiv 0.47\ 2^{-\frac{2\mathcal{N}}{3}} \left[2^{\frac{4\mathcal{N}}{3}} - 1\right]^{\frac{1}{2}}, \tag{2.4}$$

where u_j^{Δ} is the velocity field associated with the smallest resolved scale Δ, and where the number of cascade steps in the subgrid field is given by

$$\mathcal{N} \equiv \log_2(\Delta/\lambda_\nu). \tag{2.5}$$

A similar model for the concentrations of a conserved passive scalar ζ^{sgs} may be developed based on the multifractal structure of the passive-scalar dissipation field in high Reynolds number turbulence.

2.2. *Overview*

Fundamental considerations indicate that gradient-magnitude fields in turbulent flows, such as the passive-scalar energy dissipation field, given by

$$\chi(\mathbf{x}, t) \equiv -D\, \nabla\zeta \cdot \nabla\zeta(\mathbf{x}, t), \tag{2.6}$$

will display multifractal scale-similarity. This structure arises as the result of the repeated stretching and folding provided by the strain-rate and vorticity fields within turbulent flows. Such repeated stretching and folding may be represented by a stochastic multiplicative cascade, in which a scale-invariant distribution of multipliers $\mathcal{M}$ maps the given field from one scale to the next as the cascade proceeds. In one dimension, such a multiplicative cascade is given generically by

$$\mu(x) = \mu_o(x)\, 2^{\mathcal{N}} \prod_{n=1}^{\mathcal{N}} \mathcal{M}_n\,(x), \tag{2.7}$$

where the mass-density field is given by $\mu(x)$, the initial mass distribution averaged over the domain is $\mu_o(x)$ and the number of repetitions in the cascade is given by $\mathcal{N}$.

A number of prior experimental studies have confirmed that the passive-scalar dissipation field in high Reynolds-number turbulence does in fact exhibit multifractal scale-similarity over inertial-range scales (Prasad *et al.* 1988; Prasad & Sreenivasan 1989;

Frederiksen *et al.* 1997), and from this a unique distribution of scale-invariant multipliers $\mathcal{M}$ that distributes the scalar dissipation field of (2.6) according to (2.7). This multifractal structure may therefore be used to derive a model for a dynamically-passive conserved-scalar field at the subgrid scales $\zeta^{sgs}(\mathbf{x},t)$ that closes (2.1). The derivation involves representing the spatial distribution of the subgrid-scalar gradient field $\nabla\zeta^{sgs}$ by two cascades: (a) a multiplicative multifractal cascade for scalar gradient magnitudes $|\nabla\zeta^{sgs}|$ and (b) an additive decorrelation cascade for scalar-gradient orientations $\hat{\mathbf{e}}^{sgs}_{\nabla\zeta}$. This representation for the scalar gradient field is then inverted using Green's function to recover the subgrid-scalar concentrations ζ^{sgs}. The following derivation parallels in most substantial respects the derivation of the multifractal model for the subgrid velocity field u_j^{sgs} set forth in Burton & Dahm (2004*a*).

2.2.1. *The scalar-gradient magnitude cascade*

Specifying the scalar-gradient magnitude in each subgrid-scale cell first requires determining the total amount of subgrid-scalar dissipation χ^{sgs} over the LES grid cell Δ. This may be determined from Kolmogorov scaling arguments, assuming that the grid-scale Δ falls within the inertial range. Following K41 theory the scalar-dissipation spectrum $\mathcal{X}(k)$ exhibits power-law scaling in the inertial range of high Reynolds-number turbulence as

$$\mathcal{X}(k) \sim k^1. \tag{2.8}$$

Thus the total amount of subgrid-scalar dissipation can be determined by integrating the scalar-dissipation spectrum from the smallest-resolved scale k_Δ to the viscous scale k_ν, giving

$$\chi^{sgs} = \int_{k_\Delta}^{k_\nu} \mathcal{X}(k)\, dk = \kappa\, \chi^\Delta \left[\left(\frac{k_\nu}{k_\Delta} \right)^2 - 1 \right], \tag{2.9}$$

where

$$\kappa \equiv (1 - \alpha^{-2})^{-1}. \tag{2.10}$$

Using (2.9) requires estimating the average magnitude of scalar-dissipation χ^Δ in the resolved flow between filter scale Δ and some larger inertial-range scale $\alpha\,\Delta$. This may be accomplished by determining the value of the scalar field ζ^Δ, and then differentiating the field locally to determine $\nabla\zeta^\Delta$ and from this obtaining

$$\chi^\Delta \equiv -D\, \nabla\zeta^\Delta \cdot \nabla\zeta^\Delta. \tag{2.11}$$

For sufficiently small α, (2.11) provides a reasonably accurate estimate of the true nonlinear quantity χ^Δ given that the contribution of the scalar gradient magnitude at other scale ranges to the product at scale Δ will be small at high Reynolds number (see Burton & Dahm, 2004*a*).

Combining (2.9), (2.10) and (2.11), the subgrid-scalar dissipation magnitude distributed over each grid cell may be described by a three-dimensional stochastic binomial cascade, giving the amount of subgrid-scalar gradient magnitude in each inner scale cell as

$$|\nabla\, \zeta^{sgs}|(\mathbf{x},t) = \left[\chi^{sgs}\, (2^{\mathcal{N}})^3 \prod_{n=1}^{\mathcal{N}} \mathcal{M}_n(\mathbf{x},t) \right]^{\frac{1}{2}}, \tag{2.12}$$

where $\mathcal{N}$ from (2.5) is the number of cascade steps, and the multipliers $\mathcal{M}_n$ correspond to random samples from the scale-invariant distribution $P(\mathcal{M})$ for the scalar-dissipation field (*e.g.*, Frederiksen *et al.* 1997, 1998). This leads naturally to a multifractal subgrid-scalar dissipation field.

2.3. *The additive orientation cascade*

As discussed in Burton & Dahm (2004 *a*), substantial experimental and computational evidence indicates that the orientations of the subgrid velocity field are highly correlated with the orientations of the $\mathbf{u}^{\Delta}$ field. (*e.g.*, Bardina *et al.* 1983; Liu, Meneveau & Katz 1994; Domaradzki & Saiki 1997). For similar dynamic considerations, such behavior should also be apparent within the scalar-gradient field $\nabla\zeta$. To test the extent to which such correlations in fact exist, a DNS database of homogeneous isotropic turbulence including passive-scalar transport was generated, using a third-order in time, fourth-order in space finite-difference code. A series of initial simulations were made at a resolution of 128^3, corresponding to $Re_\lambda \approx 55$. These simulations were run until the field reached statistical stationarity, approximately $5t_o$, where t_o is the global eddy-turnover time. Filter width was selected at $\Delta = 2\pi/16$ approximately in the middle of the range over which log-linear behavior in the scalar-energy fluctuation field spectrum was seen to exist, as illustrated in Figure 1. Using this particular dataset, the correlations between the Δ-scale and subgrid-scale orientations of the scalar gradient field $\nabla\zeta^{\Delta/2}$ are found to be $\rho \sim 0.9$.

Using these findings, it is then possible to describe an additive decorrelation cascade by which the scalar gradient field $\nabla\boldsymbol{\zeta}$ orientations decorrelate isotropically at successively smaller scales from the local orientation of $\nabla\boldsymbol{\zeta}^{\Delta}$ at the smallest resolved scale in the LES, here denoted by the unit vector $\hat{\mathbf{e}}^{\Delta}_{\nabla\zeta}$. Between any two successive stages (n) and $(n+1)$ in the cascade, the corresponding vorticity orientations $(\hat{\mathbf{e}})_{n+1}$ and $(\hat{\mathbf{e}})_n$ thus deviate by stochastic spherical decorrelation angles θ and ϕ. Each component of the orientation unit-vector at stage $(n+1)$ is therefore determined as

$$(\hat{e}_i)_{n+1} \;=\; (\hat{e}_i)_n \;+\; f_i(\phi,\theta)_{n+1}, \tag{2.13}$$

where $f_1(\phi,\theta) = \sin\phi\,\cos\theta$, $f_2(\phi,\theta) = \sin\phi\,\sin\theta$ and $f_3(\phi,\theta) = \cos\phi - 1$. Since isotropy requires θ to be uniformly distributed, the θ dependence will vanish trivially in the expectation value $\langle\nabla\boldsymbol{\zeta}^{sgs}\rangle$ of the stochastic subgrid vorticity field. The ϕ distribution on the other hand should be strongly correlated with the multiplier values $\mathcal{M}$.

Based on the above considerations, a scalar-gradient intermittency factor $\mathcal{I}^s$ can be defined from a correlation between $\nabla\boldsymbol{\zeta}^{sgs}$ and $\nabla\boldsymbol{\zeta}^{\Delta}$ as

$$\mathcal{I}^s \;=\; \int_{\mathbf{x}'} \nabla\boldsymbol{\zeta}^{sgs}\cdot\nabla\boldsymbol{\zeta}^{\Delta}\; d^3\,\mathbf{x}' \;\Bigg/\; \int_{\mathbf{x}'} |\nabla\boldsymbol{\zeta}^{sgs}|\,|\nabla\boldsymbol{\zeta}^{\Delta}|\, d^3\,\mathbf{x}' \,. \tag{2.14}$$

The subgrid scalar gradient field $\nabla\boldsymbol{\zeta}^{sgs}$ after $\mathcal{N}$ cascade steps can then be expressed in terms of $\mathcal{I}^s(\mathcal{N})$ as

$$\nabla\boldsymbol{\zeta}^{sgs}(\mathbf{x},t) \;=\; |\nabla\boldsymbol{\zeta}^{sgs}|\,\left(\mathcal{I}^s(\mathcal{N})\,\hat{\mathbf{e}}^{\Delta}_{\nabla\zeta}(\mathbf{x},t) \;+\; (1-\mathcal{I}^s)\sum_{n=1}^{\mathcal{N}}\boldsymbol{\delta}^s_n\right) \tag{2.15}$$

where $\boldsymbol{\delta}^s_n$ are the scalar-gradient field decorrelation increments in the orientation cascade. Owing to the stochastic nature of both the multiplier values $\mathcal{M}_n$ in the magnitude cascade and the decorrelation increments $\boldsymbol{\delta}^s_n$ in the orientation cascade, the subgrid scalar gradient $\nabla\boldsymbol{\zeta}^{sgs}(\mathbf{x},t)$ is a stochastic field. From (2.15) its expectation value $\langle\nabla\boldsymbol{\zeta}^{sgs}\rangle$ involves correlations between the multipliers $\mathcal{M}_n$ and the increments $\boldsymbol{\delta}^s_n$. If the effect of

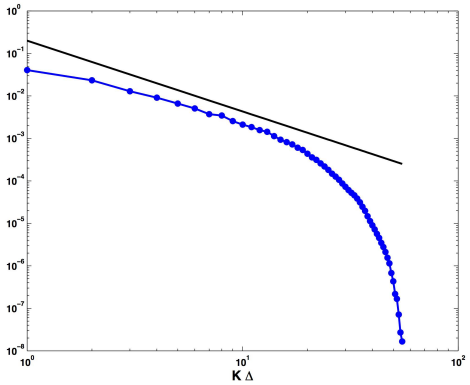

FIGURE 1. Scalar energy spectrum $\mathcal{S}(k) = frac12\zeta^2(k)$ from DNS database with $N = 128^3$ and $Re_\lambda \approx 55$ used for the *a priori* study of the multifractal model in section 4, below. Inertial-convective range scaling of $\mathcal{S}(k) \sim k^{-5/3}$ is apparent over at least one decade of length scales in the dataset.

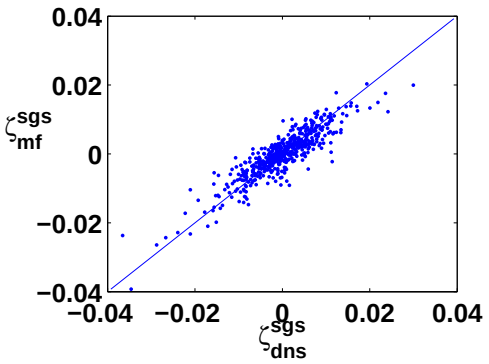

FIGURE 2. Scatterplot of DNS vs. model values for the filtered scalar concentrations $\overline{\zeta^{sgs}}$, from DNS database of $N = 128^3$ and $Re_\lambda \approx 55$. This is an important initial test for the validity of the model set out in (2.24) and (2.25). Model correlations are found to be $\rho \geq 0.90$ for the particular conditions considered.

these correlations is taken to be negligible, then

$$\langle \nabla\boldsymbol{\zeta}^{sgs} \rangle \;=\; \mathcal{I}^s(\mathcal{N})\,\langle |\nabla\boldsymbol{\zeta}^{sgs}| \rangle\,\hat{\mathbf{e}}^{\Delta}_{\nabla\zeta} \;+\; (1-\mathcal{I}^s)\,\langle |\nabla\boldsymbol{\zeta}^{sgs}| \rangle \sum_{n=1}^{\mathcal{N}} \langle \boldsymbol{\delta}^s_n \rangle\,. \tag{2.16}$$

Furthermore, if the decorrelation cascade is isotropic, then the expectation value of the increments in (2.16) vanishes, giving from (2.12)

$$\langle \nabla\boldsymbol{\zeta}^{sgs} \rangle \;=\; \mathcal{I}^s(\mathcal{N})\,\left(2^{\mathcal{N}}\right)^{\frac{3}{2}} \left\langle (\mathcal{M}_1 \cdots \mathcal{M}_{\mathcal{N}})^{\frac{1}{2}} \right\rangle\,(\chi^{sgs})^{1/2}\;\;\hat{\mathbf{e}}^{\Delta}_{\nabla\zeta}, \tag{2.17}$$

where χ^{sgs} comes from (2.9).

2.3.1. *Inversion using Green's Function*

The expectation value of the subgrid scalar concentrations $\langle \zeta^{sgs} \rangle$ is obtained from the corresponding subgrid scalar-gradient field $\langle \nabla\boldsymbol{\zeta}^{sgs} \rangle$ in (2.17) via the Green's function approach, as

$$\langle \zeta^{sgs} \rangle = \nabla \cdot \frac{1}{4\pi} \int_{\mathbf{x}'} \langle \nabla\boldsymbol{\zeta}^{sgs} \rangle\;\frac{1}{|\mathbf{x}-\mathbf{x}'|}\,d\mathbf{x}'\,. \tag{2.18}$$

Since the distribution $P(\mathcal{M})$ of the multipliers in $\langle \nabla\boldsymbol{\zeta}^{sgs} \rangle$ is the same everywhere, from (2.17) and (2.18) the expectation value becomes

$$\langle \zeta^{sgs} \rangle \;=\; \mathcal{I}(\mathcal{N})\,\left(2^{\mathcal{N}}\right)^{\frac{3}{2}} \left\langle (\mathcal{M}_1 \cdots \mathcal{M}_{\mathcal{N}})^{\frac{1}{2}} \right\rangle \left(\frac{\chi^{sgs}}{\chi^{\Delta}}\right)^{\frac{1}{2}} \nabla \cdot \frac{1}{4\pi} \int_{\mathbf{x}'} (\chi^{\Delta})^{1/2}\,\hat{\mathbf{e}}^{\Delta}_{\nabla\zeta}\;\frac{1}{|\mathbf{x}-\mathbf{x}'|}\,d\mathbf{x}'\,. \tag{2.19}$$

The Green's function integral in (2.19) is simply ζ^{Δ}, giving with (2.5) and (2.9)

$$\langle \zeta^{sgs} \rangle \;=\; \mathcal{I}(\mathcal{N})\;2^{\frac{3}{2}\mathcal{N}} \left\langle \mathcal{M}^{\frac{1}{2}} \right\rangle^{\mathcal{N}} \left[2^{\mathcal{N}}-1\right]^{\frac{1}{2}} \sqrt{\kappa}\;\zeta^{\Delta}\,, \tag{2.20}$$

where we have also made use of the fact that the multipliers are statistically independent.

From (2.20) the subgrid scalar concentration values ζ^{sgs} can be written as

$$\zeta_i^{sgs}(\mathbf{x},t) \approx \mathcal{I}^s(\mathcal{N})\,\mathcal{A}^s(\mathcal{N})\sqrt{\kappa}\,\zeta^{\Delta}(\mathbf{x},t) \tag{2.21}$$

where

$$\mathcal{A}^s \equiv 2^{\frac{3}{2}\mathcal{N}}\left\langle \mathcal{M}^{\frac{1}{2}}\right\rangle^{\mathcal{N}}\left[2^{\mathcal{N}}-1\right]^{\frac{1}{2}}. \tag{2.22}$$

2.3.2. *Final form of model*

The intermittency factor $\mathcal{I}^s$ from (2.14) that appears in (2.21) is implied by the required Re_Δ-independence of ζ^{sgs} as $Re_\Delta \to \infty$. As correspondingly $\mathcal{N} \to \infty$ this requires

$$\mathcal{I}^s(\mathcal{N}) \approx C_{\mathcal{I}^s}\,2^{-2\mathcal{N}}\left\langle \mathcal{M}^{\frac{1}{2}}\right\rangle^{-\mathcal{N}}. \tag{2.23}$$

The associated proportionality constant $C_{\mathcal{I}^s}$ should be universal, and can be obtained from *a priori* testing using the DNS data discussed above, with the result that $C_{\mathcal{I}^s} \approx 0.3$. Together with the multifractal model for the subgrid velocity components of (2.3) and (2.4), this gives the multifractal model for the subgrid scalar flux vector σ_j^* as

$$\sigma_j^* \approx \mathcal{D}\,\overline{\overline{u}_j\,\zeta^{\Delta}} + \mathcal{B}\,\overline{u_j^{\Delta}\,\overline{\zeta}} + \mathcal{B}\,\mathcal{D}\,\overline{u_j^{\Delta}\,\zeta^{\Delta}}, \tag{2.24}$$

where

$$\mathcal{D} \equiv 0.39\;2^{-\frac{2\mathcal{N}}{3}}\left[2^{\frac{4\mathcal{N}}{3}}-1\right]^{\frac{1}{2}} \tag{2.25}$$

where $\mathcal{B}$ is given by (2.4), and where $\mathcal{N}$ is from (2.5). This involves only quantities available from the resolved scales of the flow, thus closing the subgrid-scalar flux term in the passive-scalar transport equation in (2.1) and (2.2).

3. Numerical implementation of the passive-scalar flux model

Each of the filtered product terms appearing in (2.24) and (2.1) is calculated using an explicit Legendre box filter, following the method presented in Burton & Dahm (2004*a*). In brief, this approach approximates each velocity component and scalar term by a three-dimensional Legendre expansion, which for the resolved velocity component field is given as

$$\overline{u}_j(\mathbf{x}) \approx \sum_{l,m,n} a_{lmn}\,\Phi_l(x)\,\Phi_m(y)\,\Phi_n(z) \equiv \mathcal{G}_j(\mathbf{x}), \tag{3.1}$$

and for the Δ-scale velocity component as

$$u_j^{\Delta}(\mathbf{x}) \approx \sum_{l,m,n} b_{lmn}\,\Phi_l(x)\,\Phi_m(y)\,\Phi_n(z) \equiv \mathcal{H}_j(\mathbf{x}). \tag{3.2}$$

Legendre expansions for the resolved and Δ-scale passive-scalar concentrations, $\mathcal{G}^s$ and $\mathcal{H}^s$, are defined similarly. The filtered products in the subgrid-scalar flux vector σ_j^* in (2.24) are then explicitly evaluated by integrating over the grid cell volume as

$$\overline{\overline{u}_j\zeta^{\Delta}} \approx \frac{1}{\Delta^3}\int_{\Delta^3}\mathcal{G}_j(\mathbf{x})\,\mathcal{H}^s(\mathbf{x})\,d^3\mathbf{x} \tag{3.3}$$

$$\overline{u_j^{\Delta}\overline{\zeta}} \approx \frac{1}{\Delta^3}\int_{\Delta^3}\mathcal{H}_j(\mathbf{x})\,\mathcal{G}^s(\mathbf{x})\,d^3\mathbf{x} \tag{3.4}$$

$$\overline{u_j^{\Delta}\,\zeta^{\Delta}} \approx \frac{1}{\Delta^3}\int_{\Delta^3}\mathcal{H}_j(\mathbf{x})\,\mathcal{H}^s(\mathbf{x})\,d^3\mathbf{x}, \tag{3.5}$$

and similarly the explicit filter on the inertial term in (2.1) is evaluated as

$$\overline{\overline{u}_j\,\overline{\zeta}} \;\approx\; \frac{1}{\Delta^3}\int_{\Delta^3} \mathcal{G}_j(\mathbf{x})\,\mathcal{G}^s(\mathbf{x})\,d^3\mathbf{x}. \tag{3.6}$$

Equations (2.24) – (3.6) allow evaluation of σ_j^* and the nonlinear term $\overline{\overline{u}_j\,\overline{\zeta}}$ in (2.1), and together provide a complete statement of the multifractal subgrid-scale model for large-eddy simulation of the mixing of a conserved passive-scalar.

4. *A priori* evaluation of the multifractal passive-scalar flux model

Because multifractal modeling of the subgrid passive scalar concentrations, like the related velocity model, attempts to replicate the actual structure of the unknown subgrid field, its performance in actual large-eddy simulations can be accurately assessed by *a priori* testing, in which model values are compared with DNS or expermental data from one realization of the given flow field.† As a result, the model for the filtered scalar flux term of the previous section was first tested in the *a priori* sense against the DNS database described above.

The filtered scalar fields $\overline{\zeta}$ supplied to the subgrid-scale model were first used to construct the subgrid scalar concentration fields from (2.21), and the resulting fields then filtered at the scale Δ using the Legendre box filter to give the filtered subgrid scalar concentration components $\overline{\zeta^{sgs}}$. As can be seen by the scatterplot in Figure 2, the model values agree well with the DNS data, with correlations of $\rho \approx 0.90$. For purposes of an actual large eddy simulation, the most relevant *a priori* comparison is of the subgrid scalar flux vector σ^* from (2.24) and the complete scalar flux vector σ^T, where

$$\sigma^T \;\equiv\; \overline{\overline{u}_j\,\overline{\zeta}} \;+\; \mathcal{D}\,\overline{\overline{u}_j\zeta^{\Delta}} \;+\; \mathcal{B}\,\overline{u_j^{\Delta}\overline{\zeta}} \;+\; \mathcal{B}\mathcal{D}\,\overline{u_j^{\Delta}\,\zeta^{\Delta}}. \tag{4.1}$$

As indicated in Figure 3, the subgrid scalar σ^* correlations exceed $\rho \geq 0.9$ (*right column*), while for the complete scalar flux term σ^T correlations exceed $\rho \geq 0.995$ (P*left column*). The latter is the most relevant measure for an actual LES, since the complete σ^T is necessary to solve the passive-scalar transport equation, and since each term in (4.1) is implicated in energy transfer to the subgrid scales. Finally, corrrelations were also examined for the subgrid scalar energy production field, given by

$$\mathcal{P}^s \equiv \left[\overline{\overline{u}_j\,\overline{\zeta}} + \mathcal{D}\,\overline{\overline{u}_j\zeta^{\Delta}} + \mathcal{B}\,\overline{u_j^{\Delta}\overline{\zeta}} \;+ \mathcal{B}\mathcal{D}\,\overline{u_j^{\Delta}\,\zeta^{\Delta}}\right]\,\frac{\partial\overline{\zeta}}{\partial x_j}. \tag{4.2}$$

As illustrated in Figure 4, correlations for that portion of the subgrid-scalar energy transfer due to σ^* in (2.2) exceed $\rho = 0.90$, while for the complete scalar-energy production field given by (4.2) correlations exceed $\rho \geq 0.995$. This indicates that at least for the conditions considered here the multifractal model recovers the details of the spatial distribution of $P^s(\mathbf{x},t)$ with extremely high accuracy.

5. *A posteriori* evaluation of the multifractal passive-scalar flux model.

The multifractal model for the flux of a filtered passive scalar was next tested in actual large-eddy simulations of forced, periodic, homogeneous isotropic turbulence with passive

† This is in contrast to eddy-viscosity methods, which cannot recover the details in the subgrid stress or energy production fields, and thus in which *a priori* tests provide little guidance about the model's performance in an actual simulation.

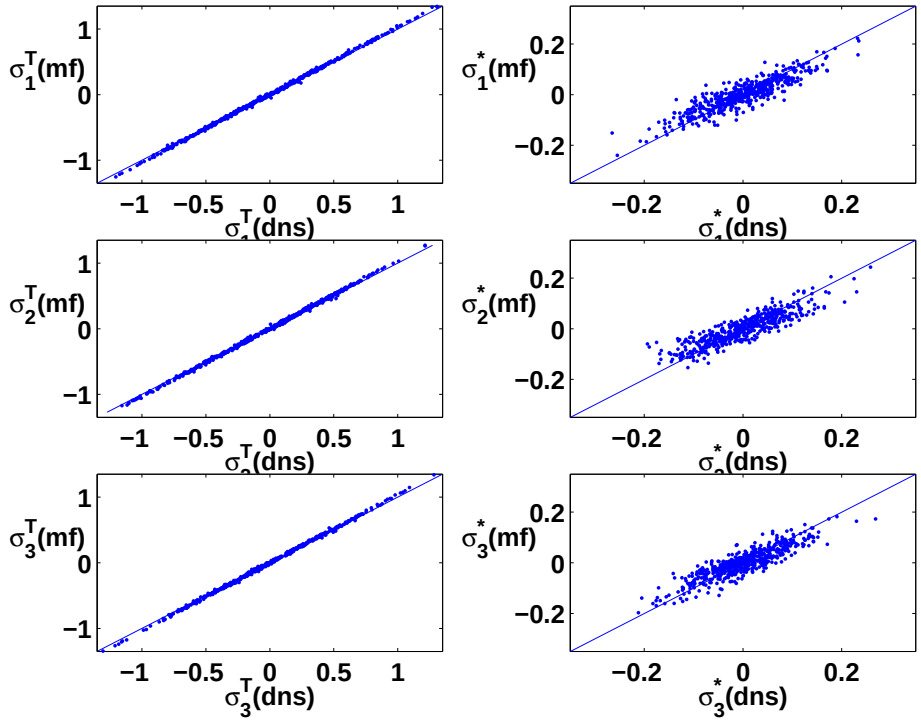

FIGURE 3. Scatterplot comparisons between DNS and model values for the full scalar flux σ^T given by (4.1), and that portion of the scalar flux involving the subgrid scalar concentrations ζ^{sgs} given in (2.2). Graphic indicates that correlations for σ_j^* exceed $\rho = 0.9$ (*right column*), while correlations for σ_j^T exceed $\rho = 0.995$ (*left column*). This indicates that the multifractal model produces exceedingly accurate representations of the scalar-inertial stress $\sigma^T(x,t)$ needed to solve the filtered passive-scalar transport equation of (2.1).

scalar mixing. The simulations were conducted at a resolution of $N = 32^3$, at $Re_\lambda \approx 160$ and a Schmidt number of $Sc = 1$. Details of the computational setup as well as the use of the backscatter limiter are given in Burton & Dahm (2004*b*).

The simulations were initiated by allowing an initial velocity field, randomized as to phase and with a kinetic energy spectrum scaling of $k^{-5/3}$ to reach a statistically stationary state, after which the passive-scalar field was introduced to the calculation. Various initialized states for the passive-scalar field have been implemented including a double-delta p.d.f. with concentrations near 0 and 1, where $\beta(\zeta) \equiv 0.5\,\delta(\zeta - 0) + 0.5\,\delta(\zeta - 1)$. Other simulations have been initialized with a normally distributed scalar concentration field in which the scalar energy field exhibited the traditional inertial-convective range power law scaling of $\mathcal{S}(k) \sim k^{-5/3}$. The simulations were then run to varying final times t_f where $4t_o \leq t_f \leq 20t_o$, where t_o is the global eddy-turnover time. Forcing for both the velocity and scalar fields is obtained by rescaling wave modes $|k| \leq 2$, so that a constant energy is maintained in those wavemodes throughout the simulation. Statistical measures were taken thereafter at a frequency of $2t_o$ to guarantee statistically independent samples of the flow field.

As illustrated in the time-evolution of the simulation in Figure 5 (*top*), the multifractal passive-scalar model runs stably over nearly 12 eddy turnover times, indicating that

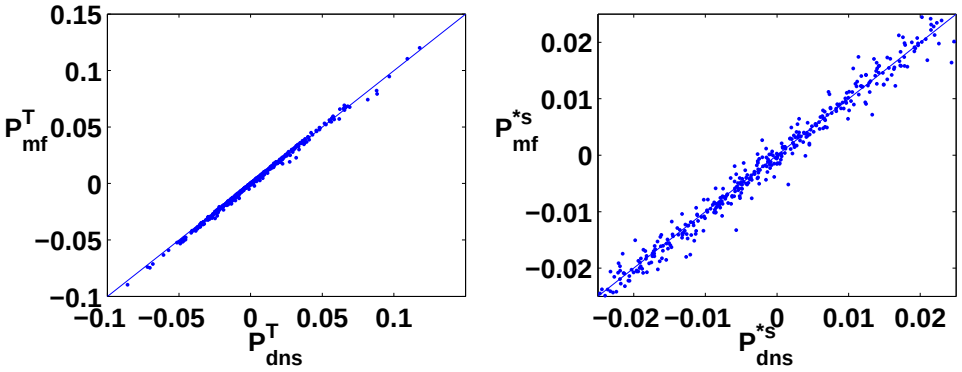

FIGURE 4. Scatterplots of scalar-energy production field comparing DNS values against the multifractal model given in (4.2). Graphic indicates that for the present DNS data, correlations exceed $\rho = 0.9$ for $\mathcal{P}^{*s}$ and $\rho = 0.995$ for the complete scalar energy production field $\mathcal{P}^{s}$ in (4.2) (*left and right columns respectively*).

the backscatter limiter for both the kinetic energy and scalar energy fields properly maintains resolved kinetic and scalar energies at physically realistic levels. In addition, the model reproduces the well-known result for flows where $Sc \approx 1$, that in the inertial-convective range, the scalar energy spectrum exhibits a power law scaling where $\zeta^2(k) \sim k^{-5/3}$, as shown in Figure 5 (*bottom*). This is a hallmark of high Reynolds number turbulence, as are the deviations from the Gaussian distribution for the skew components of the velocity gradient tensor illustrated in Figure 6. There it is evident that the flow field exhibits significant intermittency indicated by the log-linear tails of the velocity gradient magnitudes distributions. In addition Figure 7 illustrates the probability density functions for the scalar energy production (*left*) and kinetic energy production fields (*right*).

6. Future plans

6.1. *LES of passive-scalar mixing with mean scalar gradient*

Additional analysis must first be completed for the current case of forced periodic homogeneous isotropic turbulence. This includes evaluation of the scalar, scalar gradient and scalar dissipation distributions generated by LES with the multifractal model for given initial conditions of the scalar and velocity fields. Since the initial fields are randomized, it is crucial to establish within rigorous statistical bounds the performance of the model by running a number of simulations with constant parameters using different realizations of the given initial fields.

Thereafter, the model will be evaluated in the more sensitive and well-documented problem of high Reynolds-number turbulent mixing in the presence of a mean scalar gradient. Several DNS studies have been conducted of this flow regime (*e.g.,* Overholt & Pope 1996) and will provide the data against which the LES simulations will be compared. With a mean scalar gradient, the resolved-scale scalar energy equation is given by

$$\frac{1}{2}\frac{\partial}{\partial t}\overline{\zeta}^2 + \frac{\partial}{\partial x_j}\left(\overline{\zeta}\,\overline{u_j\,\zeta} + \overline{\zeta}\,\overline{u_j\,\alpha x_k} - D\,\overline{\zeta}\,\frac{\partial\overline{\zeta}}{\partial x_j}\right) = \left(\overline{u_j\,\zeta} + \overline{u_j\,\alpha x_k}\right)\frac{\partial\overline{\zeta}}{\partial x_j} - D\,\frac{\partial\overline{\zeta}}{\partial x_j}\,\frac{\partial\overline{\zeta}}{\partial x_j}, \tag{6.1}$$

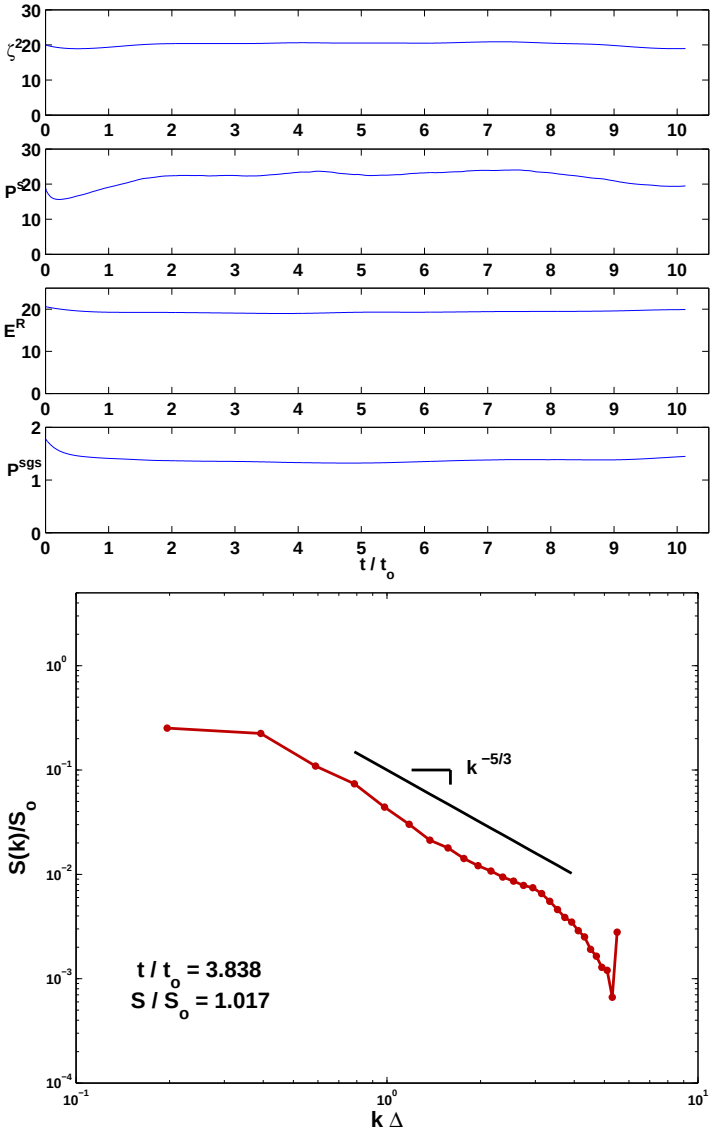

FIGURE 5. Large-eddy simulation with passive scalar mixing for $N = 32^3$, $Re_\lambda \approx 160$ and $Sc = 1$. (*Top frame, top to bottom:*) Evolution of resolved passive-scalar energy $\overline{\zeta}^2$, passive-scalar energy production P^s, resolved kinetic energy E^R, and kinetic energy production P^{sgs}, indicating that with the multifractal model and backscatter limiter the simulation runs stably to long integrated times. (*Bottom frame:*) Energy spectrum for resolved scalar concentrations $\frac{1}{2}\overline{\zeta^2}$, exhibiting the power law scaling $S(k) \sim k^{-5/3}$ characteristic of the inertial-convective range in high-Reynolds number turbulent scalar mixing.

where the total scalar field is expressed as

$$\zeta\,(\mathbf{x},t) \;=\; \left(\,\overline{\zeta} \;+\; \zeta^{sgs}\,\right)(\mathbf{x},t) \;+\; \alpha\, x_k\,, \tag{6.2}$$

and where α represents the mean scalar gradient imposed in the k-th component direc-

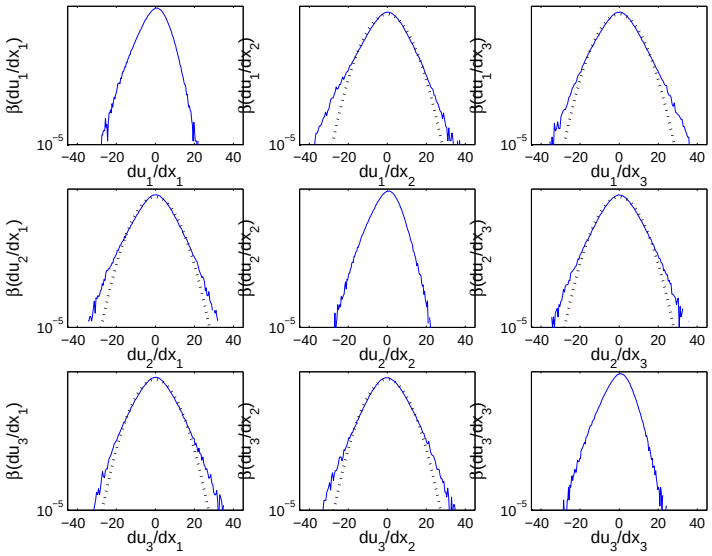

FIGURE 6. Probability distributions of the velocity gradient tensor from the LES of passive scalar mixing at $N = 32^3$ and $Re_\lambda \approx 160$ and $Sc = 1.0$. Note the significant deviation of the off-diagonal p.d.f.s from the Gaussian (dotted) indicating that the model is recovering significant intermittency seen in the resolved scales in real high Reynolds number turbulent flow, some three to four orders of magnitude smaller than the mean.

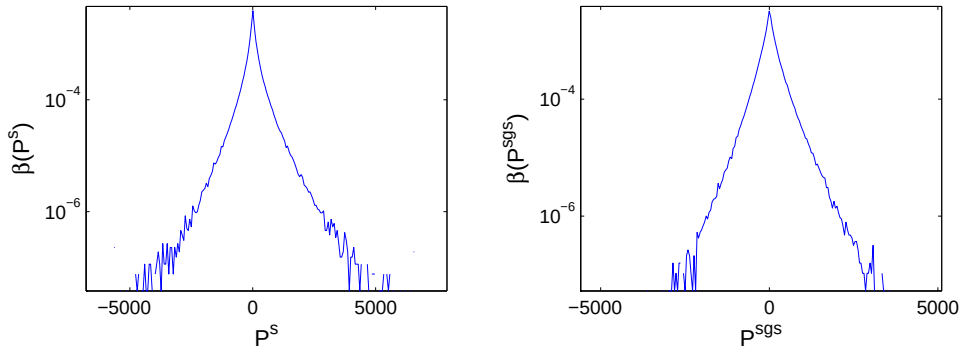

FIGURE 7. Probability distributions of the scalar energy production (*left*) and kinetic energy production (*right*) for LES using multifractal model developed in this paper.

tion. From (6.1), it is apparent that the mean gradient α imposes an additional source term on the scalar energy equation by the scalar flux working against the mean scalar gradient (Overholt & Pope 1996). Prior DNS studies have shown that the normalized scalar variance, dissipation time ratio, and the ratio of subgrid-scalar energy production to total scalar-energy dissipation all become independent of Reynolds number above $Re_\lambda \geq 180$. In addition, it has been demonstrated that the skewness of the scalar gradient in the direction of the imposed mean gradient may grow smaller with increasing Schmidt number (Yeung *et al.* 2002). The accuracy of the multifractal model will therefore be evaluated in the context of these well-established measures of passive-scalar mixing in fully developed turbulent flow with a mean scalar gradient.

6.2. *LES of free round jet with passive-scalar mixing*

Finally, the multifractal model will be incorporated into the modified JETCODE described in Burton (2004), so that the present modeling approach may be evaluated in the context of simulations involving passive-scalar mixing in a free round turbulent jet. Since turbulent jets are encountered in many practical combustion applications such as turbines, furnaces, and rocket engines, this configuration will provide an important test of the efficacy of multifractal modeling for a variety of practical turbulence modeling problems using large-eddy simulation.

REFERENCES

Bardina, J., Ferziger, J. H. & Reynolds, W. C. 1983 Improved turbulence models based on large eddy simulation of homogeneous, incompressible, turbulent flows. *Technical Report TF-19*, Thermosciences Div., Stanford University, Stanford, CA.

Burton, G. C. 2004 Large-eddy simulation of a free round jet using multifractal subgrid-scale modeling. *Annual Research Briefs 2004* Center for Turbulence Research, NASA/Stanford University.

Burton, G. C. & Dahm, W. J. A. 2004*a* Multifractal subgrid-scale modeling for large-eddy simulation. Part 1: model development and *a priori* testing. *Submitted to Phys. Fluids.*

Burton, G. C. & Dahm, W. J. A. 2004*b* Multifractal subgrid-scale modeling for large-eddy simulation. Part 2: backscatter limiting and *a posteriori* evaluation. *Submitted to Phys. Fluids.*

Domaradzki, J. A. & Saiki, E. M. 1997 A subgrid-scale model based on the estimation of unresolved scales of turbulence. *Phys. Fluids* **9** 2148-2164.

Frederiksen, R. D., Dahm, W. J. A. & Dowling, D. R. 1997 Experimental assessment of fractal scale similarity in turbulent flows. Part 3. Multifractal scaling. *J. Fluid Mech.* **338** 127-155.

Frederiksen, R. D., Dahm, W. J. A. & Dowling, D. R. 1998 Experimental assessment of fractal scale similarity in turbulent flows. Part 4. Effects of Reynolds and Schmidt numbers. *J. Fluid Mech.* **377** 169-187.

Liu, S., Meneveau, C. & Katz, J. 1994 On the properties of similarity subgrid-scale models as deduced from measurements in a turbulent jet. *J. Fluid Mech.* **275** 83-119.

Overholt, M. R. & Pope, S. B. 1996 Direct numerical simulation of a passive scalar with imposed mean gradient in isotropic turbulence *Phys. Fluids* **8** 3128-3148.

Prasad, R. R., Meneveau, C. & Sreenivasan, K. R. 1988 The multifractal nature of the dissipation field of passive scalars in fully turbulent flows. *Phys. Rev. Lett.* **61** 74-77.

Sreenivasan, K. R. & Prasad, R. R. 1989 New results on the fractal and multifractal structure of the large Schmidt number passive scalars in fully turbulent flows. *Physica D* **38** 322-329.

Yeung, P. K., Xu, S. & Sreenivasan, K. R. 2002 Schmidt number effects on turbulent transport with uniform mean scalar gradient *Phys. Fluids* **14** 4178-4191.